

Co-variability of smoke and fire in the Amazon basin



Amit Kumar Mishra, Yoav Lehahn, Yinon Rudich*, Ilan Koren*

Department of Earth and Planetary Sciences, Weizmann Institute of Science, Rehovot 76100, Israel

HIGHLIGHTS

- Joint statistical analysis of fire and smoke is conducted in the Amazon basin.
- Analysis shows strong inter-annual correlation between smoke (AOD) and fire (FC).
- Spatial homogenization of smoke are found over the basin on a seasonal time scale.
- MODIS-AODs have a stronger correlation with fire properties than AERONET-AODs.
- Provided optimal spatial-temporal scales for AOD data for different applications.

ARTICLE INFO

Article history:

Received 4 November 2014

Received in revised form

1 March 2015

Accepted 5 March 2015

Available online 6 March 2015

Keywords:

Smoke

Fire

AOD

MODIS

AERONET

ABSTRACT

The Amazon basin is a hot spot of anthropogenically-driven biomass burning, accounting for approximately 15% of total global fire emissions. It is essential to accurately measure these fires for robust regional and global modeling of key environmental processes. Here we have explored the link between spatio-temporal variability patterns in the Amazon basin's fires and the resulting smoke loading using 11 years (2002–2012) of data from the Moderate Resolution Imaging Spectroradiometer (MODIS) and the Aerosol Robotic Network (AERONET) observations. Focusing on the peak burning season (July–October), our analysis shows strong inter-annual correlation between aerosol optical depth (AOD) and two MODIS fire products: fire radiative power (FRP) and fire pixel counts (FC). Among these two fire products, the FC better indicates the amount of smoke in the basin, as represented in remotely sensed AOD data. This fire product is significantly correlated both with regional AOD retrievals from MODIS and with point AOD measurements from the AERONET stations, pointing to spatial homogenization of the smoke over the basin on a seasonal time scale. However, MODIS AODs are found better than AERONET AODs observation for linking between smoke and fire. Furthermore, MODIS AOD measurements are strongly correlated with number of fires $\sim 1^0$ – 2^0 to the east, most likely due to westward advection of smoke by the wind. These results can be rationalized by the regional topography and the wind regimes. Our analysis can improve data assimilation of satellite and ground-based observations into regional and global model studies, thus improving the assessment of the environmental and climatic impacts of frequency and distribution variability of the Amazon basin's fires. We also provide the optimal spatial and temporal scales for ground-based observations, which could be used for such applications.

© 2015 Elsevier Ltd. All rights reserved.

1. Introduction

Smoke aerosols from natural and anthropogenic fire are significant modulator of climate (Turco et al., 1990; Kaufman and Fraser, 1997; Schultz et al., 2003; van der Werf et al., 2008; Boucher et al., 2013) through their direct interaction with incoming and outgoing

radiation (Davidi et al., 2009; Leibensperger et al., 2012 and references therein) and their ability to affect cloud microphysics and therefore hydrological processes (Andreae et al., 2004; Koren et al., 2004; 2008; Stevens and Feingold, 2009; Tao et al., 2013; Altartaz et al., 2014; Rosenfeld et al., 2014). The spatial and temporal variations in the properties of smoke aerosol particles lead to high uncertainties in global and regional climate radiative forcing calculations (Boucher et al., 2013). This is also true for smoke in the Amazon basin, which is a hot spot of anthropogenically-driven biomass burning (Cochrane, 2003; Aragao et al., 2007). Biomass burning is a large source of particulate matter during the burning

* Corresponding authors.

E-mail addresses: Yinon.Rudich@weizmann.ac.il (Y. Rudich), ilan.koren@weizmann.ac.il (I. Koren).

season (June–November) in the Amazon Basin (Martin et al., 2010), which accounts for 15% of total global fire emissions on average (van der Werf et al., 2010). The major part of the emissions originates from agriculture crop residue burning (Reinhardt et al., 2001; Ribeiro, 2008; Uriarte et al., 2009) and deforestation fires along the borders of the Amazon forest, known as the arc of deforestation (Morton et al., 2008). However, atmospheric transport patterns lead to smoke spatial distribution that can be very different than the distribution of the actual fire sources (Freitas et al., 2005).

The availability of fire products from satellites [e.g. the Moderate Resolution Imaging Spectroradiometer (MODIS), Advanced Very High Resolution Radiometer, and Along Track Scanning Radiometer etc.] enable new dimensions of research, that include long term global and regional quantitative studies of biomass-burning (Wooster et al., 2003; Ichoku and Kaufman, 2005; Ichoku et al., 2008; Kaiser et al., 2012; Schroeder et al., 2014), emission estimates of organic and black carbon (Vermote et al., 2009), elucidating biomass burning patterns and trends (Duncan et al., 2003; Giglio et al., 2006a, 2006b; Koren et al., 2007; Ichoku et al., 2008; Hovee et al., 2012; Hyer et al., 2013), and quantifying the potential of smoke injection heights using sub-pixel information of fire properties (Peterson et al., 2013, 2014). Satellite-derived fire pixel counts (FC) or fire radiative powers (FRP) with different parameterizations are generally used to synthesize a variety of smoke emissions inventories. These include the Global Fire Assimilation System, which estimates emissions by converting MODIS-derived FRP into dry matter burnt and fire constituents using land-cover dependent conversion factors (Kaiser et al., 2012; Remy and Kaiser, 2014). The Brazilian Biomass Burning Emission Model uses satellite derived-FC with a different emission parameterization to synthesize emission inventories of biomass burning species (Freitas et al., 2009; Longo et al., 2010). These smoke emission inventories are needed for simulating smoke transport and for accurately representing radiative impacts in global climate models (GCM) and regional chemical transport models (CTM). Although making best use of available datasets, there are large uncertainties associated with the output of these atmospheric models due to uncertainties in absolute emission fluxes and other unknown or not yet fully understood processes.

One way to reduce these uncertainties may be the assimilation of satellite-derived aerosol optical depth (AOD, derived from smoke) in conjugation with FC or FRP data into established GCMs and CTMs. An alternative method could be provided to validate these model products regarding their prescribed fires and estimated biomass burning fluxes. However, for such applications, one must know the link between fire (FC, FRP) and smoke loading.

In this study, a joint statistical analysis of fire and smoke loading was conducted for the burning seasons for 2002–2012 using MODIS and Aerosol Robotic Network (AERONET) observations. Specifically, this study addresses the following questions (1) How does smoke loading scale with FC and FRP? (2) How does this association vary as a function of spatial and temporal scale? (3) How do the basin-wide atmospheric dynamics affect the observed co-variability?

2. Study region and data analysis

Combined statistics of fire and smoke loading are analyzed for the Amazon basin during the fire season (June–November) between 2002 and 2012. A large domain over the deforestation arc (4°S – 18°S , 70°W – 44°W) is used as a primary region of interest (ROI) in this study (Fig. 1). The ROI mainly constitute deforestation-fire, Savana (Cerrado)-fire and crop-residue burning during the Amazonian dry season (Castellanos et al., 2013).

Monthly (MYD14CMH, $0.5^{\circ} \times 0.5^{\circ}$ spatial resolution) and eight-

day mean (MYD14C8H, $0.25^{\circ} \times 0.25^{\circ}$ spatial resolution) of MODIS (Aqua) Collection 5 level 3 climate modeling grid (CMG) fire products are used to retrieve overpass-corrected fire pixel counts, mean cloud fraction, cloud-and-overpass-corrected fire pixel counts and mean fire radiative power (Justice et al., 2002; Kaufman et al., 1998, 2003; Giglio et al., 2006a; 2006b; Giglio, 2013). The CMG fire products are planned to facilitate the MODIS fire information into GCMs and CTMs. These fire products are obtained from <http://modis-fire.umd.edu/pages/ActiveFire/ActiveFire.html> & <ftp://fuoco.geog.umd.edu/modis/C5/cmg/>. The traditional 'gridded fire counts' are corrected for multiple satellite overpass and missing values, which are termed as 'overpass-corrected fire pixel counts' for each grid cell (Giglio et al., 2006b). In general, high cloud cover during the burning season hinders the detection of small fires and hence the observed FC may be smaller than the actual FC. Therefore, 'cloud-and-overpass-corrected fire pixel counts' are computed for each grid cell, which is the ratio of 'overpass-corrected fire pixel counts' to '1 – mean cloud fraction' (Giglio et al., 2006b). The cloud-and-overpass-corrected fire pixel counts for those grid cells where 'mean cloud fraction = 1' are denoted zero. The 'cloud-and-overpass-corrected fire pixel counts' will be used in this study as FC. The calculation of FRP requires the information about brightness temperature of fire pixels and background (non-fire) brightness temperature in the immediate vicinity of the fire, using the $4 \mu\text{m}$ channel (Kaufman et al., 2003; Giglio, 2013). However, the information about background brightness temperature is sometimes unavailable in the neighborhood of high cloud cover and very large fires. The fire pixels which fall in above mentioned cases and those that are detected at scan angle above 40° are not included in mean FRP calculation. Detailed information on CMG fire products and their estimation methodology could be found in Kaufman et al. (2003), Giglio et al. (2006b) and Giglio (2013).

Apart from high cloud cover, other limitations to the fire detection process from the MODIS observations also exist (Giglio et al., 2003; 2006b; Philip, 2007). Many small agricultural fires are missed in the detection process because they are too small to raise the brightness temperature of the pixel. Therefore, it is difficult to distinguish it from the background brightness temperature. The number of missed detections increases away from nadir, as the pixel size increases from 1 km to 8–10 km. In addition, there are gaps between the MODIS swaths in the equatorial regions, which also contribute to the number of missed detections. More details on fire detection limitations from MODIS observations can be found elsewhere (Giglio et al., 2003; Philip, 2007; Giglio, 2013). In addition, the level 3 CMG products provide mean FRP at coarse spatial resolutions ($0.5^{\circ} \times 0.5^{\circ}$ & $0.25^{\circ} \times 0.25^{\circ}$) as compared to level 2 products ($1 \text{ km} \times 1 \text{ km}$), which could reduce the signal from the largest and most intense fires. Ichoku et al. (2008) have shown that the decrease in spatial resolution of the sensors tends to underestimate the relative FRP. However, the mutual high correlations between these sensors indicate that the general variation in FRP is well captured, irrespective of the spatial resolution.

AOD at 550 nm is retrieved from MODIS (Aqua) Collection 5.1 level 3 global aerosol products (monthly mean, eight-day mean and daily) (Remer et al., 2008; Levy et al., 2007). MODIS AOD products are retrieved on $1^{\circ} \times 1^{\circ}$ spatial resolutions. In order to compare with AOD product, the spatial resolution of MODIS fire product is reduced to $1^{\circ} \times 1^{\circ}$ using the methodology given in Giglio (2013), i.e. FCs are sum of individual pixels and FRPs are average of individual pixels, weighted by their individual FC.

Due to discontinuity in availability of AERONET-derived daily level 2 data for longer time period (2002–2012), AERONET level 1.5 (cloud corrected) AOD₅₀₀ from 4 sites, Abracos_Hill (AH), Alta_Floresta (AF), Ji_Parana_SE (JPSE) and Rio_Branco (RB) are used in this study (Holben et al., 1998). Due to limited availability of data

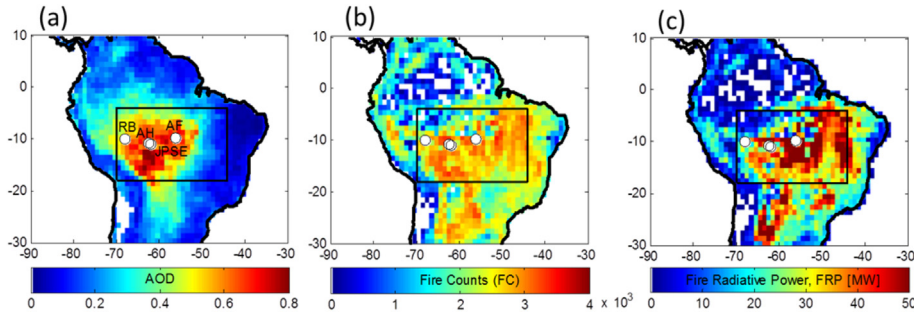


Fig. 1. 11 yr (2002–2012) seasonal (July–October) mean composite of (a) aerosol optical depth (AOD) (b) fire counts (FC), and (c) fire radiative power (FRP) over the Amazon Basin. FC is presented as multiple of 10^3 . Rectangular boxes represent the region of interest (ROI) over the Amazon. The AERONET sites used in this study are shown by white colored circle with respective site names in Fig. 1a.

from sites AH (2002–2005) and JPSE (2006–2012) and their close proximity (within ~50 km), combined measurements of AH and JPSE will be used and termed AH in this study. The mean AERONET term will be used for mean values of AODs from all AERONET sites. The AERONET sites are shown in Fig. 1a. AERONET AOD values were calculated as hourly means at ± 30 min around Aqua-MODIS overpass. All the correlation coefficients in this study are calculated by creating a single time series from 2002 to 2012 for the burning season for different temporal scales of data.

3. Association between fire and smoke loading

Fig. 1 shows 11 yr (2002–2012) seasonal (July–October) mean composite of (a) AOD (b) FC and (c) FRP over the Amazon Basin. Although smoke is a direct product of fire, the spatial distribution of FC and FRP as compared to smoke coverage across the basin clearly shows advection effects. The eastern part of the basin shows large fire concentration but relatively small smoke loading.

Fig. 2 presents the gridded correlations between AOD and FC for the peak burning season (July–October) from 2002 to 2012 over the

Amazon Basin. Columns represent different AODs (individual sites, mean AERONET, and MODIS) and rows refer the temporal scale of data, used in the calculation of the correlations. The gridded correlation maps are calculated on the basis of AOD product (from each AERONET site, mean AERONET and MODIS-AOD) and MODIS-derived FC/FRP data for all MODIS grid boxes during the peak burning season (July–October). For AERONET data, the correlations at each grid point for each specific site are calculated using AERONET’s AOD and grid specific MODIS-derived FC/FRP. Similarly, the correlations are calculated at each grid point between co-located grid specific MODIS-derived AOD and MODIS-derived FC/FRP.

Fig. 2 reveals a common feature that as we move from higher to lower temporal resolution of data (from up to down), the correlation increases substantially for all AOD’s type (will be discusses in Section 4). Fig. 2 also demonstrates that any single AERONET site can capture basin wide fire during the burning season and this capability is enhanced for combined measurement of all AERONET sites (fourth column from left in Fig. 2). All three sites present strongly anisotropic and inhomogeneous shape of area with moderate to high correlations ($R > 0.5$). These strong correlations show

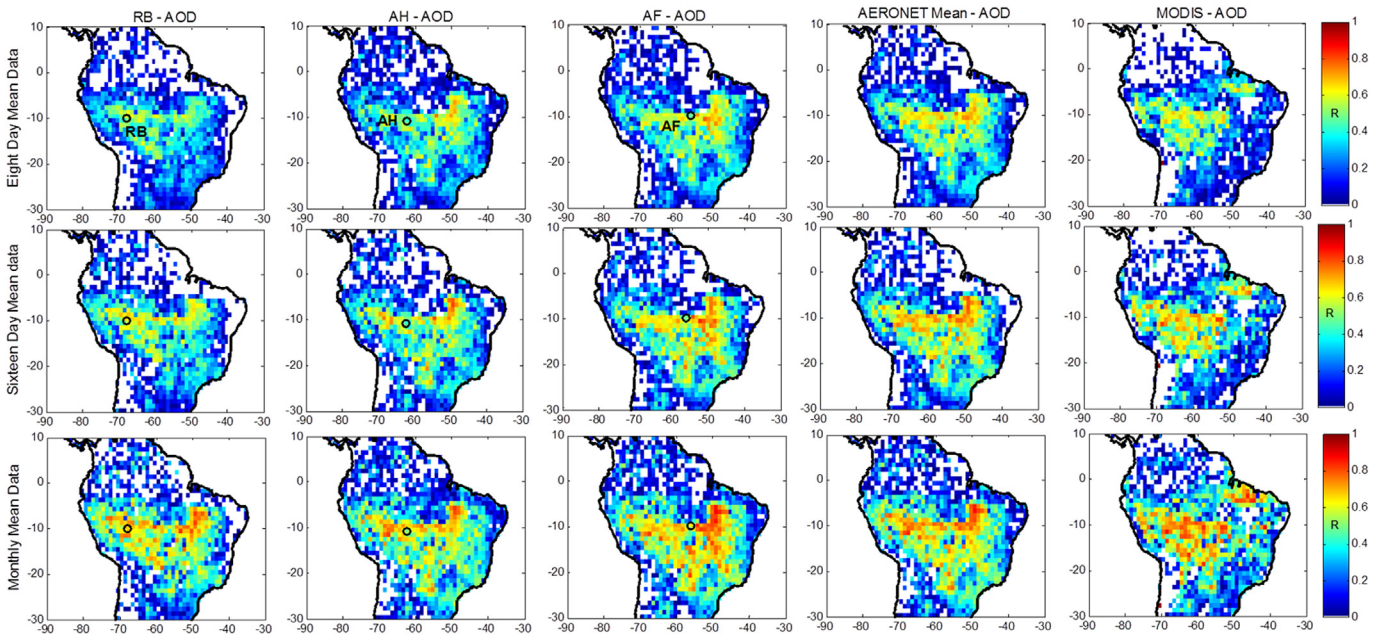


Fig. 2. Gridded correlations (R) between AOD and FC for the peak burning season (July–October) from 2002 to 2012 over the Amazon Basin. The columns represent different AOD products (individual sites, mean AERONET and MODIS) and the rows refer the temporal scale of data, used in calculation of R. The AERONET sites are depicted by black colored circle on respective plots.

that observations from these sites may be used to represent the measurement for much larger areas for initialization of assimilation-based CTMs (Sandhu et al., 2005).

The differences in correlations for different AERONET sites could be rationalized by considering their location with respect to fire sources, convoluted with the transport of smoke in the basin (will be discussed in Section 4). MODIS-derived AODs also show a strong correlation with FC (right-most lower panel in Fig. 2) and shows a similar spatial pattern as AERONET. Very low values and missing patches of correlations that can be seen in the eastern part of basin (between -7°N to -10°N and -50°E to -40°E) are caused by MODIS AOD artifacts over the bright surface (Hsu et al., 2004). The location mismatch between the highest AOD and FC (Fig. 1) and the strong spatial variability of correlation suggests that atmospheric dynamics plays an important role in regulating the linkage between the fields (will be discussed in Section 4).

We plot monthly averaged MODIS-AOD versus FC and FRP over the ROI for 2002–2012 (Fig. 3a and b). Similar plot for mean AERONET AOD vs. FC and FRP is given in Fig. S1. The best associations in Fig. 3 are between (a) FC and AOD in a linear way with $R = 0.90$, and (b) FRP and AOD in a logarithmic way with $R = 0.70$ ($R_{\log(\text{AOD})}$ vs. R_{AOD} vs. FRP). The results indicate that AOD have a linear relationship with FC and a non-linear relationship with FRP. Therefore, all the correlations are calculated against $\log(\text{AOD})$ data in case of the FRP data. The logarithmic association of FRP with AOD could be explained by exponential saturation of FRP with increasing FC (Fig. S2b). FC shows strong linear correlation with smoke AOD relative to FRP. The saturation in FRP at higher AOD (Fig. S2a) may be related to the saturation of the mid Infra-Red (MIR) (used in FRP calculation) channel at higher temperatures (Kaufman et al., 2003; Roberts et al., 2005). Similar type of gridded correlations (similar spatial variability to AOD vs. FC) are found between $\log(\text{AOD})$ and FRP over the Amazon basin (Fig. S3). However, it is smaller in magnitude than that from AOD vs. FC.

Fig. 3c presents the differences between the correlations found between AOD vs. FC (R_{FC}) and $\log(\text{AOD})$ vs. FRP (R_{FRP}) for the peak burning season (July–October) from 2002 to 2012 over the Amazon Basin. $R_{\text{FC}} - R_{\text{FRP}}$ is calculated for MODIS AOD for monthly mean data. Similarly, Fig. S1c represents $R_{\text{FC}} - R_{\text{FRP}}$ for mean AERONET AODs. It is evident in Fig. 3c ($R_{\text{FC}} - R_{\text{FRP}} > 0$) that the AOD association with FC is an improvement over that with FRP for the most part of the basin. The negative values of $R_{\text{FC}} - R_{\text{FRP}}$ (blue (in web version) highlighted region in Fig. 3c), observed especially over the northern part of basin are basically meaningless as this region is characterized by very few fire events. Higher correlations of AOD with FC (Fig. 3) suggest that FC, rather than FRP, better represents the smoke loading over the ROI.

The seasonality of fire occurrence and the aerosol loading over the ROI are shown in Fig. 4a. On a seasonal scale, two distinct associations between FC and AOD are observed. During the wet season (December–May), there is no real association between AOD and FC suggesting that the AOD sources are other than fires. However, during the dry and transition seasons (June–November), AOD coincides with FC. Furthermore, the peak of the monthly mean AODs coincides with the FC peak during September–October each year. Fig. 4b shows the inter-annual variation of FC and smoke loading by MODIS and AERONET measurements for the peak burning season. Both satellite-derived ($R=0.98$) and ground based-derived ($R=0.94$) AODs show strong positive correlations with FC over the ROI on the seasonal scale. This analysis reveals a remarkable aspect of the smoke-fire co-variability; i.e. the basin-scale inter-annual variability in fire is captured by the three point AERONET sites-derived AODs. It shows that the AERONET- and MODIS-derived AODs on seasonal scale can serve for validation and optimization of GCMs and/or CTMs to elucidate smoke transport

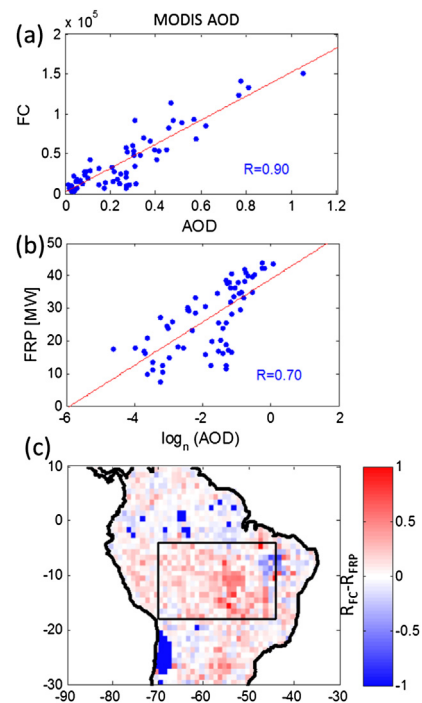


Fig. 3. Scatter plot of MODIS-derived (a) FC vs. AOD, (b) FRP vs. $\log(\text{AOD})$ and (c) the gridded correlations difference ($R_{\text{FC}} - R_{\text{FRP}}$) between AOD vs. FC (R_{FC}) and $\log(\text{AOD})$ vs. FRP (R_{FRP}) for the peak burning season (July–October) from 2002 to 2012 over the Amazon Basin. Every point in Fig. 3a and b presents the monthly mean over the ROI. Red lines represent the best linear fit on respective plots. Pearson correlation coefficients (R) are given in respective plots.

and radiative properties in the Amazon basin.

Previous studies over the Amazon basin reported such relationship, indicating that the majority of the aerosols during the burning season result from biomass burning activities (Koren et al., 2007; Torres et al., 2010; Hovee et al., 2012). These studies have also commented about the long term trend of biomass burning extent and its possible relation with a tri-national policy recommended after a severe drought in 2005 (Marengo et al., 2008). Excluding the drought year of 2007 and 2010 (Marengo et al., 2008; Lewis et al., 2011), noteworthy decreasing trend of fire and smoke loading from 2005 to 2012 (Fig. 4b) also highlights the significance of the tri-national environmental policies on fire occurrence (Brown et al., 2006; Duchelle et al., 2010; Cesario et al., 2011) as mentioned in Koren et al. (2007). However, this aspect needs further extensive analyses using at least 20 yr of AOD, fire and drought index over the basin. The higher burning activity during the drought of 2007 and 2010 has been attributed to higher number of fires relative to the drought of 2005 (Hovee et al., 2012).

4. Spatio-temporal scaling of smoke loading and fire

The relationship between FC and AOD is further studied by comparing co-variability over different temporal and spatial scales. This is done using four different temporal resolutions (eight-day, sixteen-day, monthly, and seasonal) data of AODs and FCs. Fig. 5 shows the correlation coefficients between the averaged FC with individual AERONET-derived AOD, mean-AERONET AOD and ROI averaged MODIS AOD on four different temporal resolutions. As expected the correlations improve for larger spatial and temporal domains as they lose their locality and represent more of the entire basin properties. It indicates that MODIS-AOD always outperform

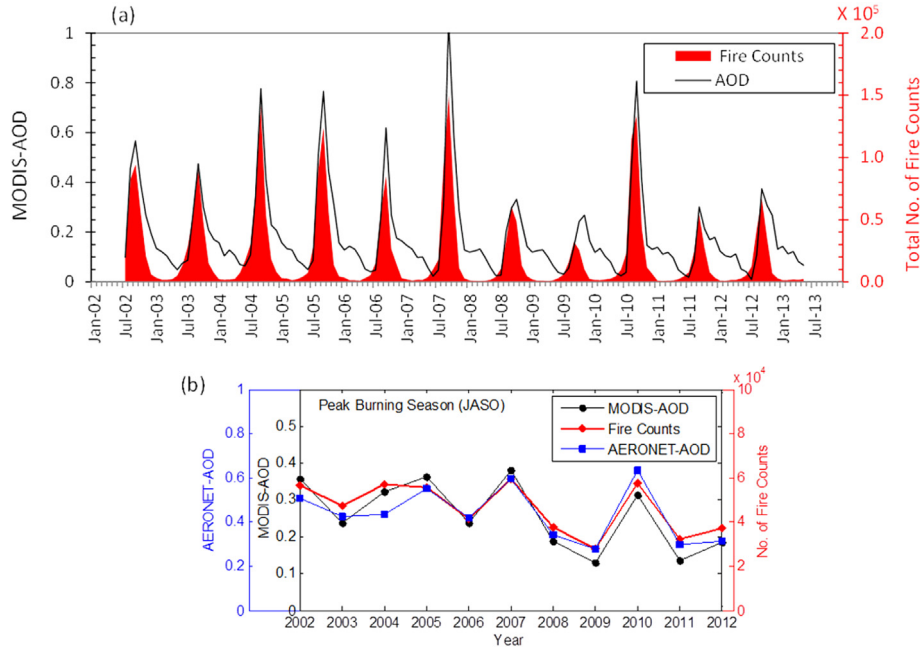


Fig. 4. (a) Monthly time series (Jan 2002–Dec 2013) of mean MODIS-AOD₅₅₀ (left axis, black) and total number of MODIS-FC (right axis, red) for the ROI over the Amazon (b) Mean MODIS AOD₅₅₀ (left axis, black), mean AERONET-AOD₅₀₀ (left axis, blue) and total MODIS-FC (right axis, red) for the ROI and peak biomass burning season (July–October) plotted as function of year. (For interpretation of the references to colour in this figure legend, the reader is referred to the web version of this article.)

the AERONET-AOD for higher spatial and temporal resolution.

Fig. 5 also shows the link between spatial to temporal scales. We can see that for the short temporal averaging, the single station data yields relatively low correlations while the average of the 3 stations improves the correlation significantly. However on the monthly and seasonal scale, we see a compensation yielding high correlations of the individual stations.

To elucidate the spatial scaling aspect, FC and MODIS-AOD around each AERONET sites are summed/averaged for four different spatial scales ($2^0 \times 2^0$ to $8^0 \times 8^0$) for different temporal resolution datasets. Table 1 shows the variation in correlation coefficients between AODs and FCs around each AERONET site for four different spatial resolutions. Three important aspects of variation can be deduced from Table 1: (1) MODIS-derived AOD shows better

correlation than AERONET-derived AOD; (2) monthly mean data shows better correlation than eight-day mean data; and (3) the correlations improve as we increase the spatial dimension for both MODIS and AERONET datasets. It is noted that the correlations in the AF site saturate when going beyond the $6^0 \times 6^0$ spatial domains for all observations. This saturation in correlation is associated with the geographical properties of the AF site that is situated in a valley-type landscape and stretching the domain beyond that valley does not increase the correlation.

Relatively high correlations have been found for co-located domains of MODIS-AODs and FCs (Fig. 2). We further investigate whether spatial lags will affect the correlations. For each time series of $1^0 \times 1^0$ FC pixels, we have investigated the MODIS AOD time series that will produce the maximal correlation within $5^0 \times 5^0$ regions around it. Fig. 6 shows (a) maximum correlations found between AODs and FC, and the positions of these maximum values for (b) longitudinal lag and (c) latitudinal lag. The ‘lags’ are spatial

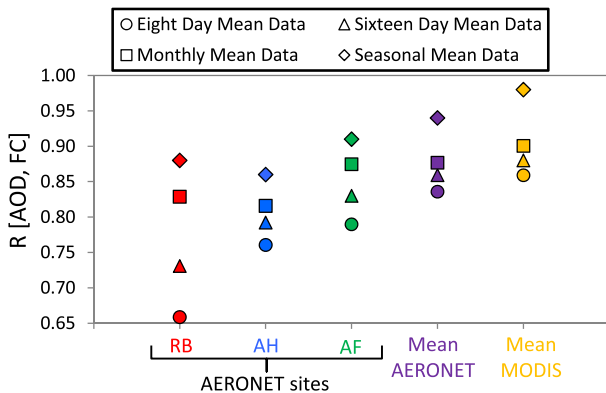


Fig. 5. The correlation coefficient ($R [AOD, FC]$) between ROI averaged MODIS-FC with AERONET sites (RB, AH and AF) AODs, mean AERONET AODs (AOD mean of RB, AH and AF), and ROI averaged MODIS AODs for entire burning season (June–November) from 2002 to 2012. Circles, triangles, squares, and diamonds represent the correlations for eight-day mean data, sixteen-day mean data, monthly mean data, and seasonal mean data, respectively. All correlations are significant at 95% confidence level.

Table 1

Variability of correlation coefficients between AOD and fire counts for different spatial and temporal resolution around each AERONET sites. The correlations are significant at 95% confidence level.

Site name	Spatial scale	$R_{\text{MODIS-AOD}}$		$R_{\text{AERONET-AOD}}$	
		Monthly mean data	Eight-day mean data	Monthly mean data	Eight-day mean data
RB2	$2^0 \times 2^0$	0.79	0.78	0.68	0.61
RB4	$4^0 \times 4^0$	0.84	0.85	0.74	0.66
RB6	$6^0 \times 6^0$	0.86	0.87	0.77	0.68
RB8	$8^0 \times 8^0$	0.89	0.89	0.8	0.7
AH2	$2^0 \times 2^0$	0.72	0.63	0.6	0.53
AH4	$4^0 \times 4^0$	0.83	0.76	0.74	0.65
AH6	$6^0 \times 6^0$	0.87	0.8	0.78	0.67
AH8	$8^0 \times 8^0$	0.89	0.82	0.8	0.68
AF2	$2^0 \times 2^0$	0.72	0.73	0.61	0.59
AF4	$4^0 \times 4^0$	0.77	0.79	0.67	0.63
AF6	$6^0 \times 6^0$	0.77	0.8	0.68	0.64
AF8	$8^0 \times 8^0$	0.77	0.8	0.68	0.64

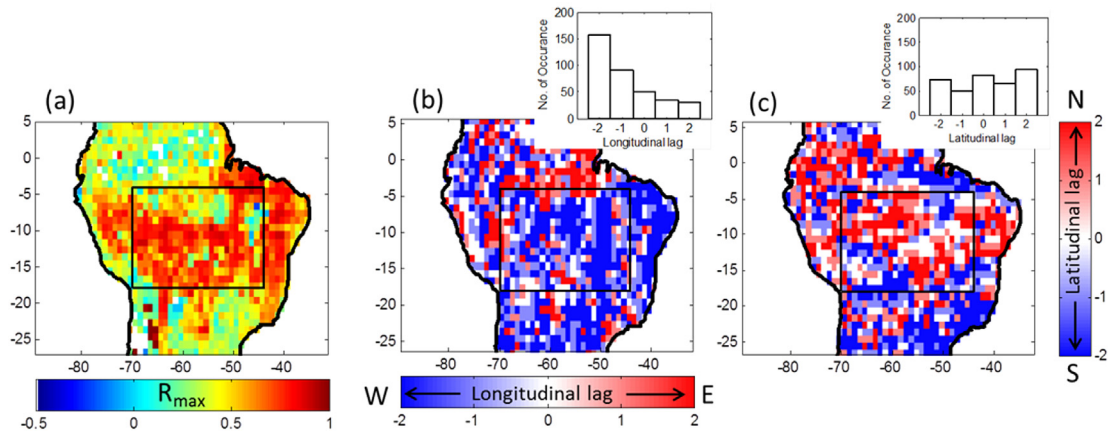


Fig. 6. Results for spatial lag analyses (a) maximum correlation coefficient (R_{max}) between FC and MODIS-AOD, and position of R_{max} for (b) longitudinal lag and (c) latitudinal lag. The inset in Fig. 6b and c represents the histogram of lag for the ROI (rectangular box).

shift in degrees latitude and longitude. If we compare Fig. 2 (15th panel, monthly co-located pixel by pixel correlation) to Fig. 6a, the enhanced correlations point out an important factor of smoke dynamics over the basin. Fig. 6b shows that the correlations improve when we move the AOD pixel by 1° or 2° westward, whereas latitudinal lag (Fig. 6c) does not show a definite pattern. The increased correlations for zonal lags are the result of westward advection of the smoke plumes by the steady winds over the basin in the dry season. This interpretation is supported by the 11 year averaged (burning seasons) wind vector (Fig. 7a). Fig. 7a shows low level easterly/south-easterly wind patterns over the Amazon basin between the equator and 20°S . Climatologically, the Amazon Basin is dominated by a high pressure area and little precipitation with light low level winds during the dry season. These conditions are generally associated with the westward shift of the South Atlantic Subtropical High (SASH), the northward displacement of the Inter Tropical Convergence Zone (ITCZ) and the barrier effect of the Andes Mountains, which determines the transport of smoke plumes in the basin (Fertias et al., 2005; 2009; Ulke et al., 2011). The complete dynamics of maximum correlation as a function of longitudinal lag result from the combined topography and large-scale wind flow over the Amazon basin (Fig. 7). The position of maximum correlations are negative (i.e. eastward lag) along the edges of the Andes ($\sim 5^{\circ}\text{--}15^{\circ}\text{S}$ and $72^{\circ}\text{--}68^{\circ}\text{W}$, red (in web version) spots in Fig. 6b), which may indicate the effect of the reversal of wind direction (easterly to westerly) due to the Andes mountain range. This statistical analysis indicates the robustness of these data sets by uncovering the dynamical aspect of smoke transport in the basin

that could be used in assimilation purposes in GCMs and CTMs over the Amazon basin.

5. Conclusions

A combined statistical analysis of FC/FRP and smoke loading (AOD) in the Amazon basin during burning seasons for 2002–2012 shows a strong association between FC/FRP and AOD. The FC is a better indicator of smoke loading in the basin as compared to FRP. Our analysis reveals that inter-annual variations in FCs/FRPs are captured not only from MODIS-derived AOD, which provide information over the entire basin, but also from AOD retrieved from a single AERONET site. However, MODIS-derived AOD is a better indicator of fires as compared to point AOD measurements. The results also point out the need of spatial and temporal averaging of AERONET-AOD datasets for fire characterization in the basin. The lag analysis shows that the AOD observations are mostly the result of fires occurring on a small scale ($1^{\circ} \times 1^{\circ}$) $\sim 1^{\circ}\text{--}2^{\circ}$ eastward. These results uncover the effect of dynamics of smoke advection on link between fire and smoke in the Amazon basin.

The findings from this study could be useful for assimilating satellite-derived and ground-based AOD data into the GCMs and CTMs that use FC and FRP as indicators of basin-wide fire activity. Such assimilation would help for accurate assessment of the radiative effects of smoke aerosols in the Amazon basin. The results of this study also provide an alternative method to validate GCM's and CTM's smoke products using more realistic linking between fire and smoke from ground and satellite data.

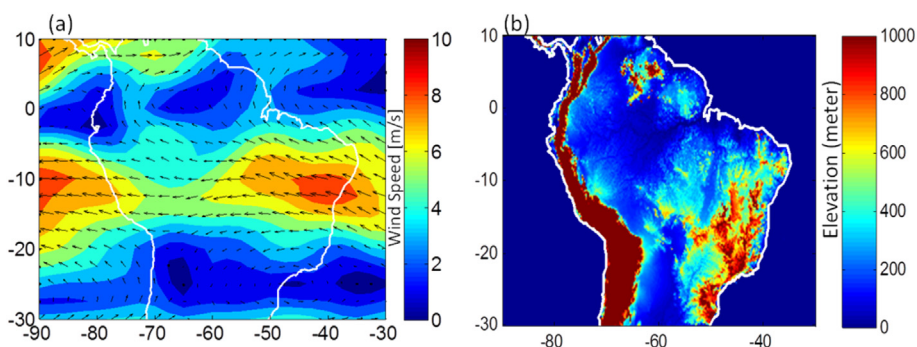


Fig. 7. (a) 11 year mean composite (for July–October, 2002–2012) NCEP/NCAR-derived vector wind at 850 hPa and, (b) Topography of the Amazon basin. Color bars represent wind speed and elevation in (a) and (b), respectively.

Acknowledgements

This research was funded by a grant from the German Israeli Science Foundation (GIF), Project no. **1136–26.8/2011**. The MODIS satellite AOD and fire datasets were obtained from the NASA Langley Research Centre Atmospheric Science Data Center. The efforts of PIs of various AERONET sites used in this study are highly appreciated.

Appendix A. Supplementary data

Supplementary data related to this article can be found at <http://dx.doi.org/10.1016/j.atmosenv.2015.03.007>.

References

- Altaratz, O., Koren, I., Remer, L.A., Hirsch, E., 2014. Review: clouds invigoration by aerosols-coupling between microphysics and dynamics. *Atmos. Res.* 140–141, 38–60. <http://dx.doi.org/10.1016/j.atmosres.2014.01.009>.
- Andreae, M.O., Rosenfeld, D., Artaxo, P., Costa, A.A., Frank, G.P., Longo, K.M., Silva-Dias, M.A.F., 2004. Smoking rain clouds over the Amazon. *Science* 303 (5662), 1337–1342.
- Aragao, L.E.O.C., Malhi, Y., Roman-Cuesta, R.M., Saatchi, S., Anderson, L.O., Shimabukuro, Y.E., 2007. Spatial patterns and fire response of recent Amazonian droughts. *Geophys. Res. Lett.* 34, L07701.
- Boucher, O., Randall, D., Artaxo, P., Bretherton, C., Feingold, G., Forster, P., Kerminen, V.-M., Kondo, Y., Liao, H., Lohmann, U., Rasch, P., Satheesh, S.K., Sherwood, S., Stevens, B., Zhang, X.Y., 2013. Clouds and aerosols. In: Stocker, T.F., Qin, D., Plattner, G.-K., Tignor, M., Allen, S.K., Boschung, J., Nauels, A., Xia, Y., Bex, V., Midgley, P.M. (Eds.), *Climate change 2013: the physical science basis. Contribution of Working Group I to the Fifth Assessment Report of the Intergovernmental Panel on Climate Change*. Cambridge University Press, Cambridge, United Kingdom and New York, NY, USA.
- Brown, I.F., Schroeder, W., Setzer, A., De Los Rios Maldonado, M., Pantoja, N., Duarte, A., Marengo, J., 2006. Monitoring fires in southwestern Amazonia rain forests. *Eos, Trans. Am. Geophys. Union* 87 (26), 253–259.
- Castellanos, P., Boersma, K.F., van der Werf, G.R., 2013. Satellite observations indicate substantial spatiotemporal variability in biomass burning NO_x emission factors for South America. *Atmos. Chem. Phys. Discuss.* 13, 22757–22793. <http://dx.doi.org/10.5194/acpd-13-22757-2013>.
- Cesario, M., Cesario, R.R., Andrade-Morraye, M., 2011. Environmental change and health impacts in Amazonia. *Hum. Health Glob. Environ. Change* 1 (1), 26–33.
- Cochrane, M.A., 2003. Fire science for rainforests. *Nature* 421, 913–919.
- Davidi, A., Koren, I., Remer, L., 2009. Direct measurements of the effect of biomass burning over the Amazon on the atmospheric temperature profile. *Atmos. Chem. Phys.* 9, 8211–8221. <http://dx.doi.org/10.5194/acp-9-8211-2009>.
- Duchelle, A., Almeyda, A., Hoyos, N., Marsik, M., Broadbent, E., Kainer, K.A., 2010. Conservation in an Amazonian tri-national frontier: patterns and drivers of land cover change in community-managed forests. In: *Proceedings of the Conference Taking Stock of Smallholder and Community Forestry: where do we go from here*.
- Duncan, B.N., Martin, R.V., Staudt, A.C., Yevich, R., Logan, J.A., 2003. Interannual and seasonal variability of biomass burning emissions constrained by satellite observations. *J. Geophys. Res. Atmos.* 108 (D2), ACH-1.
- Freitas, S.R., Longo, K.M., Dias, M.A.S., Dias, P.L.S., Chatfield, R., Prins, E., Artaxo, P., Recuero, F.S., 2005. Monitoring the transport of biomass burning emissions in South America. *Environ. Fluid Mech.* 5 (1–2), 135–167.
- Freitas, S.R., Longo, K.M., Silva Dias, M.A.F., Chatfield, R., Silva Dias, P., Artaxo, P., Andreae, M.O., Grell, G., Rodrigues, L.F., Fazenda, A., Panetta, J., 2009. The coupled aerosol and tracer transport model to the Brazilian developments on the regional atmospheric modeling system (CATT-BRAMS) – Part 1: model description and evaluation. *Atmos. Chem. Phys.* 9, 2843–2861. <http://dx.doi.org/10.5194/acp-9-2843-2009>.
- Giglio, L., 2013. MODIS Collection 5 Active Fire Product User's Guide Version 2.5. University of Maryland, College Park, MD, pp. 1–61.
- Giglio, L., Csiszar, I., Justice, C.O., 2006b. Global distribution and seasonality of active fires as observed with the terra and Aqua moderate resolution imaging spectroradiometer (MODIS) sensors. *J. Geophys. Research-Biogeosciences* 111.
- Giglio, L., Descloitres, J., Justice, C.O., Kaufman, Y., 2003. An enhanced contextual fire detection algorithm for MODIS. *Remote Sens. Environ.* 87, 273–282.
- Giglio, L., Van der Werf, G.R., Randerson, J.T., Collatz, G.J., Kasibhatla, P., 2006a. Global estimation of burned area using MODIS active fire observations. *Atmos. Chem. Phys.* 6 (4), 957–974.
- Hoeve, T.J.E., Remer, L.A., Correia, A.L., Jacobson, M.Z., 2012. Recent shift from forest to savanna burning in the Amazon basin observed by satellite. *Environ. Res. Lett.* 7 (2), 024020.
- Holben, B.N., Eck, T.F., Slutsker, I., Tanre, D., Buis, J.P., Setzer, A., Vermote, E., Reagan, J.A., Kaufman, Y.J., Nakajima, T., Lavenu, F., Jankowiak, I., Smirnov, A., 1998. AERONET—A federated instrument network and data archive for aerosol characterization. *Remote Sens. Environ.* 66, 1–16. [http://dx.doi.org/10.1016/S0034-4257\(98\)00031-5](http://dx.doi.org/10.1016/S0034-4257(98)00031-5).
- Hsu, N.C., Tsay, S.C., King, M.D., Herman, J.R., 2004. Aerosol properties over bright-reflecting source regions. *IEEE Trans. Geosci. Remote Sens.* 42, 557–569.
- Hyer, E.J., Reid, J.S., Prins, E.M., Hoffman, J.P., Schmidt, C.C., Miettinen, J.L., Giglio, L., 2013. Patterns of fire activity over Indonesia and Malaysia from polar and geostationary satellite observations. *Atmos. Res.* 122, 504–519.
- Ichoku, C., Kaufman, Y.J., 2005. A method to derive smoke emission rates from MODIS fire radiative energy measurements. *IEEE Trans. Geosci. Remote Sens.* 43 (11), 2636–2649.
- Ichoku, C., Giglio, L., Wooster, M.J., Remer, L.A., 2008. Global characterization of biomass-burning patterns using satellite measurements of fire radiative energy. *Remote Sens. Environ.* 112, 2950–2962.
- Justice, C.O., Giglio, L., Korontzi, S., Owens, J., Morissette, J.T., Roy, D., Descloitres, J., Alleaume, S., Petitcolin, F., Kaufman, Y., 2002. The MODIS fire products. *Remote Sens. Environ.* 83, 244–262.
- Kaiser, J.W., Heil, A., Andreae, M.O., Benedetti, A., Chubarova, N., Jones, L., Morcrette, J.-J., Razinger, M., Schultz, M.G., Suttie, M., van der Werf, G.R., 2012. Biomass burning emissions estimated with a global fire assimilation system based on observed fire radiative power. *Biogeosciences* 9 (1), 527–554.
- Kaufman, Y.J., Fraser, R.S., 1997. The effect of smoke particles on clouds and climate forcing. *Science* 277 (5332), 1636–1639.
- Kaufman, Y.J., Justice, C.O., Flynn, L.P., Kendall, J.D., Prins, E.M., Giglio, L., Ward, D.E., Menzel, W.P., Setzer, A.W., 1998. Potential global fire monitoring from EOS-MODIS. *J. Geophys. Res.-Atmos* 103 (D24), 32,215–32,238.
- Kaufman, Y.J., Ichoku, C., Giglio, L., Korontzi, S., Chu, D.A., Hao, W.M., Li, R.-R., Justice, C.O., 2003. Fire and smoke observed from the earth observing system MODIS instrument-products, validation, and operational use. *Int. J. Remote Sens.* 24 (8), 1765–1781.
- Koren, I., Kaufman, Y.J., Remer, L.A., Martins, J.V., 2004. Measurement of the effect of Amazon smoke on inhibition of cloud formation. *Science* 303 (5662), 1342–1345.
- Koren, I., Martins, J.V., Remer, L.A., Afargan, H., 2008. Smoke invigoration versus inhibition of clouds over the Amazon. *Science* 321 (5891), 946–949.
- Koren, I., Remer, L.A., Longo, K., 2007. Reversal of trend of biomass burning in the Amazon. *Geophys. Res. Lett.* 34 (20).
- Leibensperger, E.M., Mickley, L.J., Jacob, D.J., Chen, W.-T., Seinfeld, J.H., Nenes, A., Adams, P.J., Streets, D.G., Kumar, N., Rind, D., 2012. Climatic effects of 1950–2050 changes in US anthropogenic aerosols – part 1: aerosol trends and radiative forcing. *Atmos. Chem. Phys.* 12, 3333–3348. <http://dx.doi.org/10.5194/acp-12-3333-2012>.
- Levy, R.C., Remer, L.A., Mattoo, S., Vermote, E.F., Kaufman, Y.J., 2007. Second-generation operational algorithm: retrieval of aerosol properties over land from inversion of moderate resolution imaging spectroradiometer spectral reflectance. *J. Geophys. Res.* 112, D13211. <http://dx.doi.org/10.1029/2006JD007811>.
- Lewis, S.L., Brando, P.M., Phillips, O.L., van der Heijden, G.M.F., Nepstad, D., 2011. The 2010 Amazon drought. *Science* 331 (6017), 554–554.
- Longo, K.M., Freitas, S.R., Andreae, M.O., Setzer, A., Prins, E., Artaxo, P., 2010. The coupled Aerosol and tracer transport model to the Brazilian developments on the regional Atmospheric modeling system (CATT-BRAMS)—part 2: model sensitivity to the biomass burning inventories. *Atmos. Chem. Phys.* 10 (13), 5785–5795.
- Marengo, J.A., Nobre, C.A., Tomasella, J., Oyama, M.D., de Oliveira, G.S., de Oliveira, R., Camargo, H., Alves, L.M., Brown, I.F., 2008. The drought of Amazonia in 2005. *J. Clim.* 21, 495–516.
- Martin, S.T., Andreae, M.O., Artaxo, P., Baumgardner, D., Chen, Q., Goldstein, A.H., Guenther, A., Heald, C.L., Mayol-Bracero, O.L., McMurry, P.H., Pauliquevis, T., Poschl, U., Prather, K.A., Roberts, G.C., Saleska, S.R., Dias, M.A.S., Spracklen, D.V., Swietlicki, E., Trebs, I., 2010. Sources and properties of Amazonian aerosol particles. *Rev. Geophys.* 48 (2).
- Morton, D.C., DeFries, R.S., Randerson, J.T., Giglio, L., Schroeder, W., van der Werf, G.R., 2008. Agricultural intensification increases deforestation fire activity in Amazonia. *Glob. Change Biol.* 14, 2262–2275. <http://dx.doi.org/10.1111/j.1365-2486.2008.01652.x>.
- Peterson, D., Hyer, E., Wang, J., 2014. Quantifying the potential for high-altitude smoke injection in the North American boreal forest using the standard MODIS fire products and subpixel-based methods. *J. Geophys. Res. Atmos.* 119. <http://dx.doi.org/10.1002/2013JD021067>, 2013JD021067.
- Peterson, D., Wang, J., Ichoku, C., Hyer, E., Ambrosia, V., 2013. A sub-pixel-based calculation of fire radiative power from MODIS observations: 1 Algorithm development and initial assessment. *Remote Sens. Environ.* 129, 262–279.
- Philip, S., 2007. Active Fire Detection using Remote Sensing Based Polar-orbiting and Geostationary Observations: An Approach towards Near Real-time Fire Monitoring. Master in Geo-Information Science and Earth Observation for Environmental Modelling and Management. International Institute for Geo-Information Science and Earth Observation, Enschede, The Netherlands.
- Reinhardt, T.E., Ottmar, R.D., Castilla, C., 2001. Smoke impacts from agricultural burning in a rural Brazilian town. *J. Air & Waste Manag. Assoc.* 51 (3), 443–450.
- Remer, L.A., Kleidman, R.G., Levy, R.C., Kaufman, Y.J., Tanré, D., Mattoo, S., Martins, J.V., Ichoku, C., Koren, I., Yu, H., Holben, B.N., 2008. Global aerosol climatology from the MODIS satellite sensors. *J. Geophys. Res. Atmos.* 113, D14S07. <http://dx.doi.org/10.1029/2007JD009661>.
- Remy, S., Kaiser, J.W., 2014. Daily global fire radiative power fields estimation from one or two MODIS instruments. *Atmos. Chem. Phys. Discuss.* 14 (14), 20805–20844.
- Ribeiro, H., 2008. Sugar cane burning in Brazil: respiratory health effects. *Rev. Saúde*

- Pública 42 (2), 370–376.
- Roberts, G., Wooster, M.J., Perry, G.L.W., Drake, N., Rebelo, L.-M., Dipotso, F., 2005. Retrieval of biomass combustion rates and totals from fire radiative power observations: application to southern Africa using geostationary SEVIRI imagery. *J. Geophys. Res.* 110, D21111. <http://dx.doi.org/10.1029/2005JD006018>.
- Rosenfeld, D., Liu, G., Yu, X., Zhu, Y., Dai, J., Xu, X., Yue, Z., 2014. High-resolution (375 m) cloud microstructure as seen from the NPP/VIIIRS satellite imager. *Atmos. Chem. Phys.* 14, 2479–2496. <http://dx.doi.org/10.5194/acp-14-2479-2014>.
- Sandu, A., Constantinescu, E.M., Liao, W., Carmichael, G.R., Chai, T., Seinfeld, J.H., Dăescu, D., 2005. Ensemble-Based data assimilation for atmospheric chemical transport models. In: *Computational Science—ICCS 2005*. Springer, Berlin Heidelberg, pp. 648–655.
- Schroeder, W., Ellicott, E., Ichoku, C., Ellison, L., Dickinson, M.B., Ottmar, R.D., Clements, C., Hall, D., Ambrosia, V., Kremens, R., 2014. Integrated active fire retrievals and biomass burning emissions using complementary near-coincident ground, airborne and spaceborne sensor data. *Remote Sens. Environ.* 140, 719–730. <http://dx.doi.org/10.1016/j.rse.2013.10.010>.
- Schultz, M.G., Diehl, T., Brasseur, G.P., Zittel, W., 2003. Air pollution and climate-forcing impacts of a global hydrogen economy. *Science* 302 (5645), 624–627.
- Stevens, B., Feingold, G., 2009. Untangling aerosol effects on clouds and precipitation in a buffered system. *Nature* 461, 607–613.
- Tao, M., Chen, L., Wang, Z., Tao, J., Su, L., 2013. Satellite observation of abnormal yellow haze clouds over East China during summer agricultural burning season. *Atmos. Environ.* 79, 632–640. <http://dx.doi.org/10.1016/j.atmosenv.2013.07.033>.
- Torres, O., Chen, Z., Jethva, H., Ahn, C., Freitas, S.R., Bhartia, P.K., 2010. OMI and MODIS observations of the anomalous 2008–2009 Southern hemisphere biomass burning seasons. *Atmos. Chem. Phys.* 10, 2505–2513.
- Turco, R.P., Toon, O.B., Ackerman, T.P., Pollack, J.B., Sagan, C., 1990. Climate and smoke: an appraisal of nuclear winter. *Science* 247 (4939), 166–176.
- Ulke, A.G., Longo, K.M., Freitas, S.R., 2011. Biomass burning in south America: transport patterns and impacts. In: Matovic, Darko (Ed.), *Biomass – Detection, Production and Usage*. <http://dx.doi.org/10.5772/19264>, 978-953-307-492-4, InTech.
- Uriarte, M., Yackulic, C.B., Cooper, T., Flynn, D., Cortes, M., Crk, T., Uriarte, M., Yackulic, C.B., Cooper, T., Flynn, D., 2009. Expansion of sugarcane production in São Paulo, Brazil: implications for fire occurrence and respiratory health. *Agric. Ecosyst. Environ.* 132 (1), 48–56.
- van der Werf, G.R., Randerson, J.T., Giglio, L., Gobron, N., Dolman, A.J., 2008. Climate controls on the variability of fires in the tropics and subtropics. *Glob. Biogeochem. Cy.* 22, GB3028. <http://dx.doi.org/10.1029/2007GB003122>.
- van der Werf, G.R., Randerson, J.T., Giglio, L., Collatz, G.J., Mu, M., Kasibhatla, P.S., Morton, D.C., DeFries, R.S., Jin, Y., van Leeuwen, T.T., 2010. Global fire emissions and the contribution of deforestation, savanna, forest, agricultural, and peat fires (1997–2009). *Atmos. Chem. Phys.* 10, 11707–11735. <http://dx.doi.org/10.5194/acp-10-11707-2010>.
- Vermote, E., Ellicott, E., Dubovik, O., Lapyonok, T., Chin, M., Giglio, L., Roberts, G.J., 2009. An approach to estimate global biomass burning emissions of organic and black carbon from MODIS fire radiative power. *J. Geophys. Res.* Atmos. 114 (D18).
- Wooster, M.J., Zhukov, B., Oertel, D., 2003. Fire radiative energy for quantitative study of biomass burning: derivation from the BIRD experimental satellite and comparison to MODIS fire products. *Remote Sens. Environ.* 86 (1), 83–107.